Physics-based characterization of soft marine sediments using vector sensors

Oleg A. Godin, Thomas J. Deal, and Hefeng Dong

ARTICLES YOU MAY BE INTERESTED IN

Virtual head waves in ocean ambient noise: Theory and modeling
The Journal of the Acoustical Society of America **148**, 3836 (2020); https://doi.org/10.1121/10.0002926

Quantifying the contribution of ship noise to the underwater sound field
The Journal of the Acoustical Society of America **148**, 3863 (2020); https://doi.org/10.1121/10.0002922

Observation and inversion of very-low-frequency seismo-acoustic fields in the South China Sea
The Journal of the Acoustical Society of America **148**, 3992 (2020); https://doi.org/10.1121/10.0002949

Resolution dependence of rough surface scattering using a power law roughness spectrum
The Journal of the Acoustical Society of America **149**, 28 (2021); https://doi.org/10.1121/10.0002974

A seminal paper linking ocean acoustics and physical oceanography
The Journal of the Acoustical Society of America **148**, R9 (2020); https://doi.org/10.1121/10.0002761

Beam-time delay domain deconvolved scheme for high-resolution active localization of underwater targets
The Journal of the Acoustical Society of America **148**, 3762 (2020); https://doi.org/10.1121/10.0002780

ARTICLE

Physics-based characterization of soft marine sediments using vector sensors[a]

Oleg A. Godin,[1,b] Thomas J. Deal,[2] and Hefeng Dong[3]

[1]*Department of Physics, Naval Postgraduate School, 833 Dyer Road, Monterey, California 93943-5216, USA*

[2]*Naval Undersea Warfare Center Division Newport, Newport, Rhode Island 02841, USA*

[3]*Department of Electronic Systems, Norwegian University of Science and Technology, 7491 Trondheim, Norway*

ABSTRACT:

In a 2007 experiment conducted in the northern North Sea, observations of a low-frequency seismo-acoustic wave field with a linear horizontal array of vector sensors located on the seafloor revealed a strong, narrow peak around 38 Hz in the power spectra and a presence of multi-mode horizontally and vertically polarized interface waves with phase speeds between 45 and 350 m/s. Dispersion curves of the interface waves exhibit piece-wise linear dependences between the logarithm of phase speed and logarithm of frequency with distinct slopes at large and small phase speeds, which suggests a seabed with a power-law shear speed dependence in two distinct sediment layers. The power spectrum peak is interpreted as a manifestation of a seismo-acoustic resonance. A simple geoacoustic model with a few free parameters is derived that quantitatively reproduces the key features of the observations. This article's approach to the inverse problem is guided by a theoretical analysis of interface wave dispersion and resonance reflection of compressional waves in soft marine sediments containing two or more layers of different composition. Combining data from various channels of the vector sensors is critical for separating waves of different polarizations and helps to identify various arrivals, check consistency of inversions, and evaluate sediment density.
© 2021 Acoustical Society of America. https://doi.org/10.1121/10.0002975

Pages: 49–61

I. INTRODUCTION

Theoretical considerations,[1,2] laboratory measurements,[3] and results of numerous field experiments[4–16] indicate that shear wave speed in granular materials and, in particular, in unconsolidated marine sediments increases with depth z below the seafloor and is approximately proportional to a certain power z^ν of the depth as long as the composition of the materials remains unchanged. The power-law exponent ν is probably controlled by the shape and roughness of the grains. The gradient of the shear wave speed (or shear speed, for brevity) is very large at small z, and the shear speed experiences large relative changes over several meters or 10s of meters below the seafloor. Relative changes in density and compressional wave speed are much smaller, and these geoacoustic parameters can be modeled as depth-independent in a surficial layer of constant composition. Then, power-law depth-dependence of shear speed corresponds to the same power-law dependence on overburden pressure. Surficial unconsolidated sediments are "soft" in the sense that their shear rigidity and shear speed are small compared to the bulk modulus and compressional speed, respectively. For a more detailed discussion of the power-law depth-dependence of shear rigidity and additional references, see Refs. 2, 3, 17, and 18.

Soft sediments with power-law shear velocity profiles support horizontally (SH) and vertically polarized (SV) interface waves, which propagate along the seafloor with phase and group speeds on the order of the shear speed.[10,17] These interface waves are slow in the sense that their phase and group speeds are small compared to the sound speed in water and compressional speed in the bottom. The vertically polarized seismo-acoustic interface waves are usually referred to as Scholte waves.[19–22] The dispersion and polarization properties of slow Scholte waves supported by soft sediments, shape functions of these waves, and wave energy distribution between water and the seabed are all quite different from those of the Scholte waves that are supported by the interface of homogeneous fluid and solid half-spaces.[23] Moreover, dispersion properties of the vertically and horizontally polarized slow interface waves prove to be very similar,[10,17] making vector sensors indispensable for identifying the wave types. The distinctive feature of the slow interface waves, which is readily recognized in their measured dispersion curves, is a power-law dependence of their phase and group speeds on frequency. There is a one-to-one correspondence between the exponents of the power laws for the frequency dependence of phase or group speeds and the depth-dependence of the shear speed.[10,17] Observations of the interface waves are of considerable interest because their dispersion allows one to characterize geotechnical and

geoacoustic parameters of surficial sediments that are difficult to measure by other means.[7,18–20,24,25]

Vector sensors are increasingly employed in underwater acoustics to characterize seabed properties.[26–28] A rich dataset on wave propagation in the seabed[29,30] was obtained in 2007 in the course of shear wave surveying of the Gjøa oil/gas condensate field in the North Sea off Norway, where a seabed-coupled mechanical vibrator generated probing signals in the frequency band from a few to 60 Hz. A long, densely populated linear array of three-component vector sensors was employed, which helped to separate vertically and horizontally polarized waves, identify a number of interface waves, and measure their phase speeds (Fig. 1). Measured dispersion curves of the interface waves have been inverted to retrieve the shear speed profile in the upper 45–50 m of the seabed.[22,30]

There are two striking features of the vector sensor data, which have not been previously explored. First, the vertical and radial components of the measured particle velocity have sharp peaks around 38 Hz [Fig. 1(a)], which suggest some kind of a seismo-acoustic resonance.[9,31,32] Second, when plotted on the log-log scale, the dispersion curves of the interface waves exhibit two distinct slopes at large and small phase speeds [Fig. 1(b)], which suggests that the seabed contains layers with two different power-law profiles of the shear wave speed.[7,10,17] In this paper, we re-examine the experimental results reported by Dong et al.[22] with the goal of developing a simple, parsimonious geoacoustic model that qualitatively explains and quantitatively reproduces the key features of the observations. Our approach to the inverse problem is guided by a theoretical analysis of seismo-acoustic resonances and interface wave dispersion in soft sediments containing two or more layers of different composition.

The remainder of the paper is organized as follows. The experimental data underlying this work is described in Sec. II. Approximate analytic dispersion relations of interface waves supported by the seabed, which consists of two continuously stratified soft sediment layers overlaying a solid, homogeneous subbottom, are derived in Secs. III A and III B. The Wentzel–Kramers–Brillouin (WKB) approximation is employed in the derivation. The analytic dispersion relations are used in Sec. III C to find a simple geoacoustic model consistent with the interface wave observations. A physical mechanism of resonant reflection of compressional (P) waves by the seabed and geoacoustic implications of the observed resonant reflection are investigated in Sec. IV. The resulting geoacoustic model is compared to alternative models in Sec. V. Section VI summarizes our findings.

II. EXPERIMENTAL DATA

The data analyzed in this paper were acquired in a 2007 shear-wave survey[29,30] of the Gjøa field located in the Norwegian Channel in the northern North Sea off the southern coast of Norway. The water depth at the experiment site was 364 m, and the main geological interfaces at the site are flat. Surficial sediment layers are composed of soft Holocene clays deposited on glacial and glacio-marine sediments.[29,30] A massive seabed-coupled vibrator generated the seismo-acoustic wave field. The wave source was developed by the Norwegian Geotechnical Institute to efficiently generate low-frequency shear waves of different polarizations; limited P waves were also radiated by the source.[29,30] The frequency content of the probing signals generated by the source was approximately from 2 to 60 Hz with a broad maximum around 37 Hz and width of about 20 Hz at half-power level (see Fig. 5 in Ref. 29).

The signals were received on a 1-km-long ocean-bottom cable (OBC), which was deployed partially in water and partially on the seafloor in a radial direction from the source. The OBC contained 42 three-component accelerometers with 25-m spacing. To improve the resolution of short waves, a 600-m-long synthetic aperture with a much shorter 2.5-m receiver spacing was created by dragging the cable in 2.5-m steps.[29] Orientations of the three orthogonal receiver components were determined using airgun signals and used to represent the data in terms of the vertical and in-line (radial) and cross-range (tangential) horizontal components. This proved critical for proper discrimination and identification of various arrivals within the complex full field data.[22,29,30] Assuming a horizontally stratified seabed, the cross-range particle velocity is due to SH shear waves, while radial and vertical components of the particle velocity are due to SV shear waves and P waves. Detected arrivals included head waves, multiply reflected shear waves, and at least 10 modes of horizontally and vertically polarized interface, or surface, waves.[22,29,30]

Interface waves were observed at frequencies from about 2 to 20 Hz. Dispersion curves of the SH interface waves have been extracted from the cross-range components of particle acceleration measured on the synthesized aperture horizontal array, while dispersion curves of the SV interface waves have been measured using the vertical and radial components of the acceleration.[22,30] The dispersion curves are illustrated in Fig. 1(b). The interface wave dispersion curves have been previously inverted by Socco et al.[30] and Dong et al.[22] to retrieve the depth dependence of the shear wave speed in the top 40–50 m of the seabed. The seabed was modeled as a stack of homogeneous layers in these inversions.

Because of limitations on access to proprietary raw data, this paper focuses on re-analysis of the previously published[22,29,30] information on interface wave dispersion and power spectra of signals recorded by the three-component vector sensors. Available data consists of the frequency dependence of the phase speed of various interface waves [Fig. 1(b)], as retrieved by Dong et al.,[22] and power spectra of the vertical, radial, and cross-range components of the full field. The power spectra[22] averaged over multiple receivers and repeatedly emitted probing signals are shown in Fig. 1(a). For each of the vertical, radial, and cross-range components of particle velocity, the average power spectra are normalized by their respective maxima.
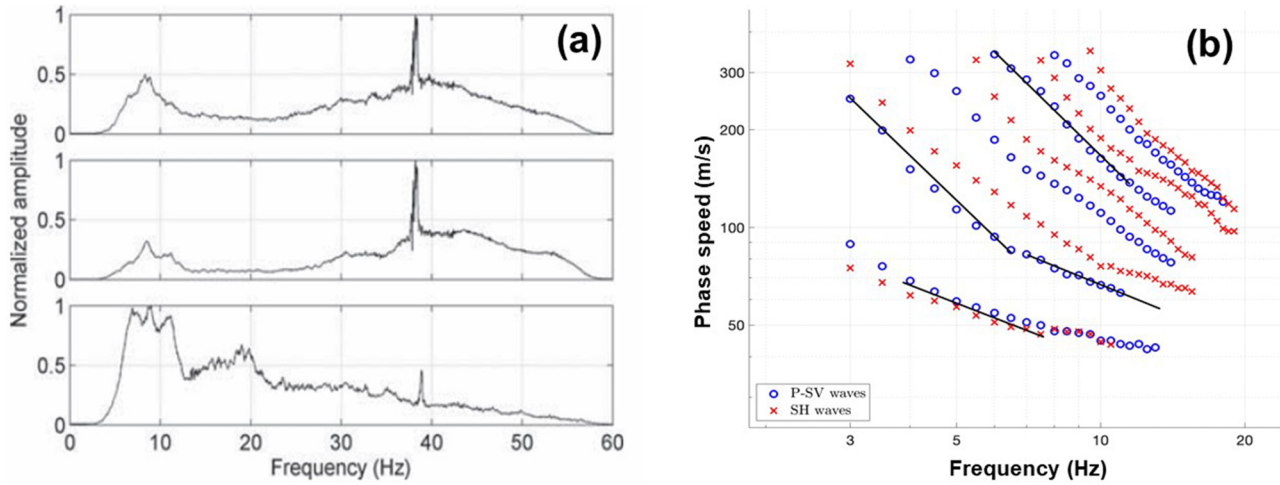
FIG. 1. (Color online) Data of a 2007 experiment in the North Sea as processed by Dong *et al.* (Ref. 22). (a) Power spectra of the vertical particle velocity (top) as well as radial (middle) and cross-range (bottom) components of the horizontal particle velocity. The spectra are averaged over 79 three-component vector sensors in a 390-m-long linear array. [Adapted from Fig. 3 in Ref. 22.] (b) Dependence of the phase speed u_n of interface waves on frequency. The phase speed values retrieved by Dong *et al.* (Ref. 22) from the experimental data are shown by crosses and circles, and plotted on log-log scale. The crosses and circles correspond to horizontally and vertically polarized waves, respectively. Superimposed straight lines represent the power-law frequency dependencies with two different exponents (two black lines each).

The main maxima of the power spectrum of the cross-range component of the field are at frequencies below 20 Hz [Fig. 1(a)]. In addition to broad low-frequency peaks below 10 Hz, which are associated with *SV* interface waves, the power spectra of the vertical and in-line components have significantly larger, narrow peaks around 38 Hz. (A much smaller peak at a similar frequency in the spectrum of the cross-range component is probably due to imperfect separation of the measured acceleration into the vertical, radial, and cross-range components resulting from uncertainties in the measurements of spatial orientation of individual vector sensors.) These sharp peaks are suggestive of a resonance phenomenon occurring in either the experimental equipment or the environment. In particular, as already mentioned, the source spectrum is maximum at about 37 Hz. However, the bandwidth of the source spectrum at half-power is at least 20 times larger than the sub-1-Hz width of the spectral peaks of the wave field [Fig. 1(a)]. We interpret the sharp spectral peaks around 38 Hz as a seismo-acoustic resonance originating from wave propagation conditions at the experimental site. It is shown in Secs. IV and V that such an interpretation is consistent with available geological information and results of inversion of the interface wave data.

III. INTERFACE WAVES

A. Asymptotic dispersion relations of horizontally polarized interface waves

Consider a model of soft marine sediments (Fig. 2), which consists of two layers with power-law shear velocity profiles:

$$c_s(z) = a_1 z^{\nu_1}, \quad 0 < z < h, \tag{1}$$

$$c_s(z) = a_2(z + z_0)^{\nu_2}, \quad h < z < H. \tag{2}$$

The layers are located between the water column at $z < 0$ and a homogeneous solid half-space (subbottom) at $z > H$. Here h is the thickness of the upper sediment layer, and H is the vertical extent of the soft sediments. Physical considerations and available observations indicate that $0 \leq \nu_{1,2} < 1$.[9,10,17] Shear and *P* wave speeds and density in the subbottom are c_{sb}, c_{lb}, and ρ_b, respectively. Sound speed and density of water near the seafloor are c_w and ρ_w; *P* wave speeds and densities in respective sediment layers are c_{l1}, ρ_1 and c_{l2}, ρ_2. For simplicity, we assume that variations of the sediment density and *P* wave speed are negligible within each soft sediment layer. We will also assume that shear speed increases steadily with depth, which implies $a_1 h^{\nu_1} \leq a_2(h + z_0)^{\nu_2}$ and $a_2(H + z_0)^{\nu_2} \leq c_{sb}$.

The increase of the shear speed c_s with depth below the seafloor creates a waveguide for shear waves. *SH* interface waves are normal modes of this waveguide. Despite the simplicity of the geoacoustic model, the wave equation
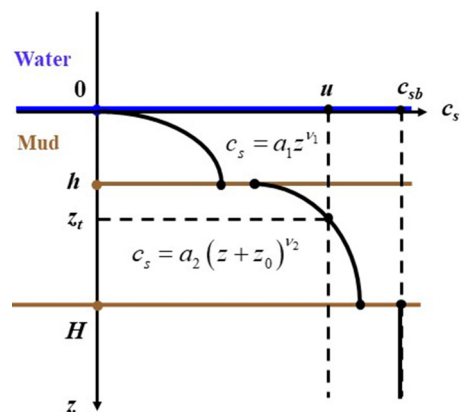

FIG. 2. (Color online) Depth dependence of the shear wave speed c_s in the seabed. Two soft sediment layers $0 < z < h$ and $h < z < H$ with power-law depth dependencies overlie a homogeneous solid subbottom.

cannot be solved analytically in terms of known mathematical functions for arbitrary values of exponents ν_1 and ν_2.[9,17] We will use a WKB-based asymptotic approach to derive the dispersion relation of the interface waves. Disregarding reflection at the interface $z = h$, the normal mode dispersion equation can be written as follows in the WKB approximation:[23]

$$V_1 V_2 \exp\left(2i\omega\varphi(z_{lb})\right) = 1, \quad \varphi(z_{lb}) = \int_0^{z_{lb}} \sqrt{c_s^{-2}(z) - u^{-2}}\, dz.$$

(3)

Here ω stands for wave frequency, V_1 and V_2 are plane-wave reflection coefficients at the upper, $z = 0$, and lower, $z = z_{lb}$, boundaries of the waveguide. The lower boundary is either the turning point $z = z_t$, where shear speed equals the phase speed u of the normal mode: $c_s(z_t) = u$, or the lower boundary $z = H$ of the soft sediment, if there are no turning points. Note that the phase integral steadily increases with u.

Introducing a new integration variable, $w = u^2/c_s^2 - 1$, reduces the phase integral $\varphi(z)$ in any layer with a power-law dependence of c_s to

$$\varphi(z_{lb}) = \frac{-1}{\nu u}\left(\frac{u^2}{a}\right)^{1/\nu} \int_{w(0)}^{w(z_{lb})} w^{1/2}(w+1)^{-1-1/\nu}\, dw.$$

This is a standard integral [see, e.g., Eq. (1.2.4.3) in Ref. 33], which can be expressed in terms of a hypergeometric function[34] for arbitrary integration limits but simplifies when one of the limits is either $w = 0$ or infinity. Note that $w = 0$ at the turning point $z = z_t$, and $w \to +\infty$ when $z \to 0$.

All normal modes are evanescent waves in the subbottom and have phase speeds $u < c_{sb}$. When $0 < u < a_1 h^{\nu_1}$, the turning point $z = z_t$ of the wave is located in the upper sediment layer at $z_t = (u/a_1)^{1/\nu_1}$. Then, integration is over the semi-infinite interval $0 < w < +\infty$ in the phase integral, and we obtain

$$\varphi(z_t) = \frac{u^{-1+1/\nu_1}}{a_1^{1/\nu_1}} \frac{\sqrt{\pi}\,\Gamma((1-\nu_1)/2\nu_1)}{2\Gamma(1/2\nu_1)}$$

(4)

in agreement with Ref. 17. Here $\Gamma(\cdot)$ is Gamma function (see Chap. 6 in Ref. 34).

When $a_1 h^{\nu_1} \leq u \leq a_2(h + z_0)^{\nu_2}$, integration in the phase integral is from $z = 0$ to $z = h$. The latter corresponds to a finite value of w. Using Eq. (1.2.4.3) in Ref. 33, we find

$$\varphi(h) = \frac{u^{-1+1/\nu_1}}{a_1^{1/\nu_1}}\left[\frac{\sqrt{\pi}\,\Gamma((1-\nu_1)/2\nu_1)}{2\Gamma(1/2\nu_1)}\right.$$
$$-\frac{1}{3\nu_1}\left(\frac{u^2}{a_1^2 h^{2\nu_1}} - 1\right)^{3/2}$$
$$\left.\times F\left(\frac{3}{2}, 1 + \frac{1}{2\nu_1}; \frac{5}{2}; 1 - \frac{u^2}{a_1^2 h^{2\nu_1}}\right)\right].$$

(5)

Here $F(A, B; C; D)$ is the hypergeometric function, also known as the Gauss hypergeometric series or $_2F_1(A, B; C; D)$ hypergeometric function (see Chap. 15 in Ref. 34).

When $a_2(h + z_0)^{\nu_2} < u < a_2(H + z_0)^{\nu_2}$, the wave has a turning point at $z_t = (u/a_2)^{1/\nu_2} - z_0$ within the lower sediment layer. Then, the phase integral is a sum of the integral in the upper sediment layer, which is given by Eq. (5), and an integral over $h < z < z_t$ in the lower sediment layer. Similar to derivation of Eq. (5), we obtain

$$\varphi(z_t) = \varphi(h) + \frac{u^{-1+1/\nu_2}}{3\nu_2 a_2^{1/\nu_2}}\left(\frac{u^2}{a_2^2(h + z_0)^{2\nu_2}} - 1\right)^{3/2}$$
$$\times F\left(\frac{3}{2}, 1 + \frac{1}{2\nu_2}; \frac{5}{2}; 1 - \frac{u^2}{a_2^2(h + z_0)^{2\nu_2}}\right).$$

(6)

Finally, when $a_2(H + z_0)^{\nu_2} \leq u < c_{bs}$, there are no turning points, and the phase integral is given by

$$\varphi(H) = \varphi(h) + + \frac{u^{-1+1/\nu_2}}{3\nu_2 a_2^{1/\nu_2}}\left[\left(\frac{u^2}{a_2^2(H + z_0)^{2\nu_2}} - 1\right)^{3/2}\right.$$
$$\times F\left(\frac{3}{2}, 1 + \frac{1}{2\nu_2}; \frac{5}{2}; 1 - \frac{u^2}{a_2^2(H + z_0)^{2\nu_2}}\right)$$
$$-\left(\frac{u^2}{a_2^2(h + z_0)^{2\nu_2}} - 1\right)^{3/2}$$
$$\left.\times F\left(\frac{3}{2}, 1 + \frac{1}{2\nu_2}; \frac{5}{2}; 1 - \frac{u^2}{a_2^2(h + z_0)^{2\nu_2}}\right)\right].$$

(7)

In the WKB approximation, the reflection coefficient from the turning point equals $V_2 = \exp(-i\pi/2)$.[23] The reflection coefficient from the boundary $z = 0$, where c_s vanishes and the shear speed gradient becomes infinite, has been found in Refs. 9 and 17 and equals

$$V_1 = \exp\left(\frac{-i\pi\nu_1}{2(1-\nu_1)}\right)$$

(8)

for *SH* waves. Using these reflection coefficients V_1 and V_2 from the dispersion Eq. (3), we find the frequency of the *SH* interface wave with a turning point in one of the sediment layers:

$$f_n = \left[\frac{n}{2} + \frac{4\nu_1 - 3}{8(1 - \nu_1)}\right] / \varphi(z_t).$$

(9)

Here $n = 1, 2, \ldots$ is the order of the interface wave. Dependence of the interface wave frequency on the phase speed enters Eq. (9) via $\varphi(z_t)$. Higher-order interface waves (normal modes) have higher frequencies at the same value of the phase velocity u and higher phase speeds at the same value of frequency. Explicit expressions for the phase integral in Eq. (9) are given by Eqs. (4) and (6) when the turning

point is located in the upper or lower sediment layer, respectively.

When there are no turning points and $a_2(H + z_0)^{\nu_2} \leq u < c_{bs}$, the wave is reflected from the boundary $z = H$. The plane wave reflection coefficient of SH waves[23] at this boundary is

$$V_2 = \exp(-2i\Phi_{SH}),$$

$$\Phi_{SH} = \arctan\left[\frac{\rho_b c_{sb}^2}{\rho_2 a_2^2 (H + z_0)^{2\nu_2}} \times \sqrt{\frac{1 - c_{sb}^{-2} u^2}{a_2^{-2}(H + z_0)^{-2\nu_2} u^2 - 1}}\right].$$

(10)

From the dispersion Eq. (3), we find

$$f_n = \left[\frac{n}{2} + \frac{5\nu_1 - 4}{8(1 - \nu_1)} + \frac{\Phi_{SH}}{2\pi}\right] \Big/ \varphi(H),$$

(11)

where the phase integral is given by Eq. (7). Finally, when $a_1 h^{\nu_1} \leq u \leq a_2(h + z_0)^{\nu_2}$, reflection occurs at $z = h$. The result is similar to Eq. (11) and differs by replacement of $\varphi(H)$ with $\varphi(h)$, Eq. (5). In addition, in the expression for the phase of the reflection coefficient in Eq. (10), one should use elastic parameters in the vicinity of the boundary $z = h$ and replace ρ_2 with ρ_1, ρ_b with ρ_2, c_{sb} with $a_2(h + z_0)^{\nu_2}$, and $a_2(H + z_0)^{\nu_2}$ with $a_1 h^{\nu_1}$ (see Fig. 2).

In the special case, where $a_1 = a_2$, $\nu_1 = \nu_2$, $z_0 = 0$, and $\nu_1 \to 0$ in Eqs. (1) and (2), we have a homogeneous solid layer with the shear speed $c_s = a_1$ that is located between homogeneous fluid ($z < 0$) and solid ($z > H$) half-spaces. In this limit, our problem reduces to the textbook setting for Love interface waves.[35] The resulting waveguide for SH waves is also equivalent to the acoustic waveguide in a homogeneous fluid layer between a rigid boundary at $z = 0$ and a homogeneous fluid half-space $z > H$.[23] In the limit $\nu_1 \to 0$, Eq. (8) gives the correct result $V_1 = 1$ for the reflection coefficient of SH waves at the solid-fluid interface,[23] and Eq. (3) gives $\varphi(H) = H\sqrt{a_1^{-2} - u^{-2}}$ for the phase integral. An inspection shows that the interface wave frequencies f_n that are predicted by Eq. (11) with $\nu_1 = 0$ agree with the textbook result[35] for the Love wave dispersion in this special case.

Equations (4) and (9) show that frequency f_n of n-th interface wave is proportional to $u^{1 - 1/\nu_1}$ when the turning point is located in the upper sediment layer. On the logarithmic scale, the slope of the dispersion curve,

$d(\ln f_n)/d(\ln u) = 1 - \nu_1^{-1}$, depends only on the shear-speed power-law exponent in Eq. (1).

When the phase speed u is much larger than the shear speed around $z = h$, the turning point is located deep in the lower sediment layer, and the vicinity of the turning point gives the main contribution into the phase integral in Eq. (3). Indeed, it follows from Eqs. (5), (6), and the equation[34]

$$\lim_{w \to \infty}\left[(w^2 - 1)^{3/2} F\left(\frac{3}{2}, 1 + \frac{1}{2\nu}; \frac{5}{2}; 1 - w^2\right)\right]$$

$$= \frac{3\sqrt{\pi}\nu\Gamma\left((1 - \nu)/2\nu\right)}{2\Gamma(1/2\nu)}$$

(12)

that under these conditions $\varphi(z_t)$ is given approximately by Eq. (4) with a_1 and ν_1 replaced with a_2 and ν_2, respectively. Then, the slope of the dispersion curves $d(\ln f_n)/d(\ln u) = 1 - \nu_2^{-1}$ is controlled by the shear-speed power-law exponent in Eq. (2).

The dispersion equations, which are derived for SH interface waves in this section and for P–SV waves in Sec. II B, describe a gradual transition between the limiting cases of the constant slope of the dispersion curves.

B. Dispersion relations of vertically polarized interface waves

Unlike SH shear waves, SV shear waves are coupled to P waves by the shear-speed gradients. In the case of the power-law shear velocity profile, the coupling is particularly strong near the seafloor $z = 0$.[17] P–SV coupling leads to the appearance of two types of slow interface waves that are supported by soft marine sediments, the fundamental mode and the main sequence modes.[10,17] The main sequence modes are uncoupled from the water column, just like SH interface waves. In the WKB approximation, the dispersion Eq. (3) of the main sequence modes differs from that for SH waves by having a different reflection coefficient[17] V_1 from the boundary $z = 0$ [cf. Eq. (8)]:

$$V_1 = \exp\left(\frac{i\pi(2 - 3\nu_1)}{2(1 - \nu_1)}\right).$$

(13)

SV reflection coefficient at interfaces, where parameters of the solid are discontinuous, is also different from the reflection coefficient Eq. (10) of SH waves. In particular, the SV reflection coefficient from the boundary $z = H$ can be written as $V_2 = \exp(-2i\Phi_{SV})$, where

$$\Phi_{SV} = \arctan\left[\frac{\sqrt{1 - \frac{u^2}{C^2}}\left[\frac{Mu^4}{4C^4} + \left(N^{-2} - M - \frac{u^2}{2C^2}\right)^2\right] - \left[N^{-2} - M + (M - 1)\frac{u^2}{2C^2}\right]^2}{\sqrt{\frac{N^2 u^2}{C^2} - 1}\left[\frac{Mv^4}{4C^4} + \left(N^{-2} - M + M\frac{u^2}{2C^2}\right)^2 - (N^{-2} - M)^2\sqrt{1 - \frac{u^2}{C^2}}\right]}\right],$$

(14)

J. Acoust. Soc. Am. **149** (1), January 2021

Godin *et al.*   53

$C = c_{sb}$, $M = \rho_b/\rho_2$, and $N = a_2^{-1}(H + z_0)^{-\nu_2}c_{sb}$. C, N, and M have the meaning of the shear speed below the boundary, the ratio of the shear speeds just below and just above the boundary, and the ratio of densities above and below the boundary, respectively. Equation (14) has been obtained from the general equation for the plane wave reflection coefficient of SV waves at solid-solid interface [see, e.g., Eq. (4.2.9) in Ref. 23] in the limit when $c_s/c_l \to 0$ in both solids.

Solving the dispersion Eq. (3) for the main sequence modes with appropriate reflection coefficients V_1 and V_2, we obtain

$$f_n = \left[\frac{n}{2} + \frac{2\nu_1 - 1}{8(1 - \nu_1)}\right] \Big/ \varphi(z_t) \qquad (15)$$

for the waves with a turning point in one of the sediment layers. Here, as in Eq. (9) for SH modes, the phase integral is given by Eq. (4), when $0 < u < a_1 h^{\nu_1}$, and by Eq. (6), when $a_2(h + z_0)^{\nu_2} < u < a_2(H + z_0)^{\nu_2}$. When $a_2(H + z_0)^{\nu_2} \leq u < c_{bs}$, waves are reflected from the boundary $z = H$, and we find

$$f_n = \left[\frac{n}{2} + \frac{3\nu_1 - 2}{8(1 - \nu_1)} + \frac{\Phi_{SV}}{2\pi}\right] \Big/ \varphi(H) \qquad (16)$$

from Eqs. (3), (13), and (14). The phase integral in Eq. (16) is given by Eq. (7). Finally, when $a_1 h^{\nu_1} \leq u \leq a_2(h + z_0)^{\nu_2}$, waves are reflected at $z = h$. The result in this case differs from Eq. (16) by substitution of $\varphi(h)$, Eq. (5), for $\varphi(H)$. In addition, $C = a_2(h + z_0)^{\nu_2}$, $M = \rho_2/\rho_1$, and $N = a_1^{-1}h^{-\nu_1}a_2(h + z_0)^{\nu_2}$ in Eq. (14) for this boundary.

The accuracy of the WKB-based asymptotic dispersion equations increases with increasing mode order,[17] and the results may not be reliable at $n = 1$. In addition, the WKB approximation gives discontinuous results and is not accurate when turning points approach and cross interfaces, where elastic parameters are discontinuous, i.e., in the vicinity of $u = a_1 h^{\nu_1}$, $u = a_2(h + z_0)^{\nu_2}$, and $u = a_2(H + z_0)^{\nu_2}$.

An alternative approach to approximating the dispersion equation, which is particularly useful for low-order modes, was developed in Ref. 17. The approach takes advantage of the availability of an exact solution, when the power-law exponent $\nu_1 = 0.5$, and builds a perturbation theory with respect to the parameter $|\nu_1 - 0.5|$ that is assumed to be small compared to unity. In marine sediments, $|\nu_1 - 0.5| < 0.5$ and is often rather small. When the shear speed in soft sediments follows the power law, by neglecting terms of second and higher order in $|\nu_1 - 0.5|$, the dispersion equation of the main sequence of $P–SV$ interface waves can be written as[17]

$$f_n = \frac{\Gamma(1/2\nu_1)a_1^{1/\nu_1}u^{1-1/\nu_1}}{2\sqrt{\pi}\Gamma((1-\nu_1)/2\nu_1)}\left[2n + (2\nu_1 - 1)\right.$$
$$\left. \times\left(\frac{3 - 2\nu_1}{2 - 2\nu_1} + \frac{1}{n} + 2n\psi(n) - 2n\ln n\right)\right], \qquad (17)$$

for arbitrary $n = 1, 2, \ldots$. Under the same assumptions, the dispersion equation of the fundamental mode is[17]

$$f_0 = \frac{(2a_1)^{1/\nu_1}u^{1-1/\nu_1}}{4\pi(1 + \rho_1/\rho_w)^{1/2\nu_1}}\exp\left[\frac{2\nu_1 - 1}{2\nu_1}(1 - \gamma)\right]. \qquad (18)$$

Here $\gamma = 0.577\,21\ldots$ is the Euler's constant, and ψ stands for the Digamma function.[34] The counterpart of Eq. (17) for SH waves is[17]

$$f_n = \frac{\Gamma(1/2\nu_1)a_1^{1/\nu_1}u^{1-1/\nu_1}}{2\sqrt{\pi}\Gamma((1-\nu_1)/2\nu_1)}\left\{2n - 1\right.$$
$$+ (2\nu_1 - 1)(2n - 1)\left[\psi(n) - \ln\left(n - \frac{1}{2}\right)\right]$$
$$\left. + \frac{2\nu_1 - 1}{2 - 2\nu_1}\right\}. \qquad (19)$$

As discussed in Ref. 17, Eqs. (17) and (19) can be used for interface waves in the case of a multi-layered seabed, provided the turning point is located in the upper soft sediment layer with a power-law shear speed profile. Equations (17) and (19) complement the asymptotic dispersion Eqs. (9) and (15) for the low-order, low-speed modes, for which the WKB-based results are either unavailable or not reliable.

C. Inversion of the interface wave dispersion data

We employ the analytical dispersion relations obtained in Secs. III A and III B as the forward model to match the measured values (Sec. II) of phase speeds of SH and SV interface waves. A nonlinear least-squares method is used to fit all the data for both wave types, simultaneously. Data from the fundamental $P–SV$ mode and the lowest order ($n = 1$) SH mode are fit to the dispersion curve for the one-layer model, i.e., Eqs. (18) and (19), respectively. Data for the higher-order modes are fit to the asymptotic dispersion relations, Eqs. (9) and (15), for the two-layer model. Simultaneously fitting the data for all interface waves to multiple theoretical dispersion curves reduces the goodness of fit for any one dispersion curve, but it ensures consistency between sediment parameters estimated across all the curves.

It is assumed in the inversion that $z_0 = 0$ in Eq. (2) and that all modes have turning points above the bottom $z = H$ of the second sediment layer. Then, the geoacoustic model contains six unknown parameters: depth h of the boundary between sediment layers, the density ratio ρ_w/ρ_1, and the power-law parameters a_1, ν_1, a_2, ν_2 in Eqs. (1) and (2). Results of the inversion, including 95% confidence bounds of the estimated parameters, are shown in Table I. The estimated value of the density ratio $\rho_w/\rho_1 = 0.537$ in Table I corresponds to the density $\rho_1 = 1910\,\text{kg/m}^3$ in the top 5.6 m of the seabed.

These parameters are used to generate a dispersion curve for each $P–SV$ and SH mode, which are drawn as solid lines in Figs. 3(a) and 3(b) for comparison with the

TABLE I. Geoacoustic inversion parameters and results.

Parameter	Unit	Estimated Value	95% Confidence Bounds
ρ_w/ρ_1	—	0.537	(0.479, 0.596)
h	m	5.57	(5.03, 6.11)
$a_1 (1m)^{\nu_1}$	m/s	46.3	(46.0, 46.7)
ν_1	—	0.288	(0.277, 0.300)
$a_2 (1m)^{\nu_2}$	m/s	24.4	(22.5, 26.3)
ν_2	—	0.710	(0.677, 0.742)

experimental data. A dotted line marks the maximum phase speed with turning points in the first layer, $u = a_1 h^{\nu_1}$, and a dashed line marks the minimum phase speed with turning points in the second layer, $u = a_2 h^{\nu_2}$. All but one of the data points for the fundamental ($n = 0$) P–SV and the first SH modes lie below these lines, justifying the use of the single-layer model for them. The dispersion curve for the mode $n = 1$ in the main sequence of P–SV modes is matched with larger errors than the other modes ostensibly because the WKB approximation becomes more accurate as mode number n increases.

Line 1 in Fig. 3(c) shows the shear speed profile as a function of depth using the parameters from Table I and Eqs. (1) and (2). Line 2 is the multi-layer model from Dong *et al.*[22] As noted in that paper, a single power-law profile is not a good fit for the data. Our two-layer model is a better fit for the data and is in reasonable agreement with the multi-layer inversion result, as discussed in more detail in Sec. V. The maximum phase speed in the data set, 350 m/s, produces the greatest turning depth, 42.5 m. These

data cannot be used to estimate shear speeds at depths greater than this.

IV. RESONANT REFLECTION OF COMPRESSIONAL WAVES

In this section we investigate the hypothesis that the strong, narrow peaks in the observed power spectra of vertical and radial components of particle velocity [Fig. 1(a)] result from the propagation conditions of P–SV waves at the site of the experiment. We offer a physical interpretation of these observations as resulting from resonantly enhanced reflection from the layered seabed, relate the resonance to the shear speed inversion results, and discuss the geoacoustic information contained in the peak frequency $f_p = 38$ Hz.

Seismo-acoustic resonances are often observed when surficial marine sediments have low shear speeds, but at much lower frequencies between about 0.3 and 7.5 Hz (see, e.g., Refs. 9, 31, and 32). Those resonances arise due to reflection of shear waves and, unlike the results illustrated in Fig. 1(a), are characterized by a large ratio of horizontal-to-vertical particle velocity amplitudes and do not exhibit a large difference between amplitudes of two orthogonal horizontal components of the particle acceleration.[9] In the North Sea experiment discussed in this paper, the peak occurs at the frequency that is considerably larger than the frequencies of observed surface waves and is, therefore, likely to be caused by P waves. The travel time $1/f$ corresponding to the peak frequency is smaller than acoustic travel time from the source on the seafloor to the ocean surface. Thus, any interference phenomena or resonances responsible for the
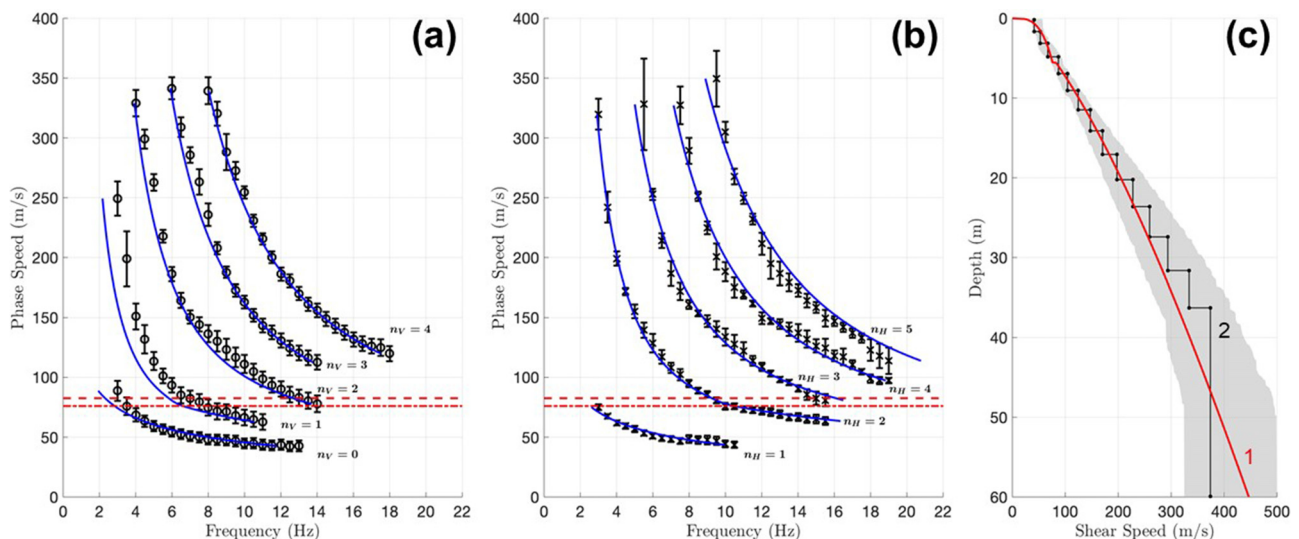

FIG. 3. (Color online) Results of an inversion of measured dispersion curves of the interface waves for depth dependence of the shear speed. (a) Comparison of the theoretical frequency dependence of the interface wave phase speed in an optimum two-layer model (solid lines) with measured phase speeds of P–SV interface waves. Error bars of measurements (Ref. 22) are shown. (b) Same for measured phase speeds of SH interface waves. Mode orders n_H and n_V of, respectively, horizontally and vertically polarized interface waves are shown in the figure. Dashed and dotted lines show inverted values of the shear speed below and above the interface $z = h$ between the soft sediment layers. (c) Comparison of the results of the parsimonious two-layer inversion (1) with an inversion in terms of a large number of homogeneous layers (Ref. 22) (2). The shaded region is the overlap of 95% confidence intervals of the shear speed profile as obtained in Ref. 22 from the separate Bayesian inversions of the dispersion curves of the horizontally and vertically polarized interface waves.

J. Acoust. Soc. Am. **149** (1), January 2021

Godin *et al.*   55

observed peak should be explained in terms of the ocean bottom properties.

Geoacoustic inversion of the measured dispersion curves of interface waves (Sec. III C) reveals a boundary between sediment layers at $h \approx 5.6$ m below the seafloor. Shear speeds just above and just below the boundary are approximately 76 and 83 m/s, respectively, which are much smaller than the P wave speeds c_l in the sediments. Surficial sediments at the experimental site are described as soft Holocene clays.[29,30] For such sediments, c_l is expected to be somewhat less than the sound speed in water near the bottom, c_w, and increase with the depth below seafloor.[7,18,36]

We will show that the power spectrum peak can be explained by the interference of P waves reflected from the seafloor and the boundary $z = h$ within sediments. Consider first a simplified geoacoustic model, where shear rigidity is neglected at $z < h$, i.e., the top layer of the bottom is approximated by a homogeneous fluid with sound speed c_{l1} [Fig. 4(a)]. The ocean bottom at $z > h$ is modeled as a homogeneous solid half-space with P wave speed c_{l2} and shear

wave speed c_{s2}. The reflection coefficient of a plane acoustic wave incident from water on the seafloor will be infinite when the following condition[23] is met:

$$V_1 V_2 \exp\left(2i\omega h \sqrt{c_{l1}^{-2} - u^{-2}}\right) = 1. \tag{20}$$

Equation (20) is similar to Eq. (3) but refers to P waves, and reflection coefficients V_1 and V_2 have a different meaning. Here V_1 and V_2 are plane-wave reflection coefficients at $z = 0$ and $z = h$ for sound waves in the layer $0 < z < h$. As in Eq. (3), V_1 and V_2 are the reflection coefficients for incidence from below and from above, respectively. In Eq. (20) u has the meaning of the phase speed of the trace of sound waves on a horizontal plane; in terms of u and wave frequency ω, the horizontal component of the wave vector ξ $= \omega/u$. Equation (20) coincides with the dispersion equation of acoustic normal modes with phase speed u in the waveguide formed by the layer $0 < z < h$.

For propagating (as opposed to evanescent) plane waves in the layer, the absolute values of reflection coefficients V_1
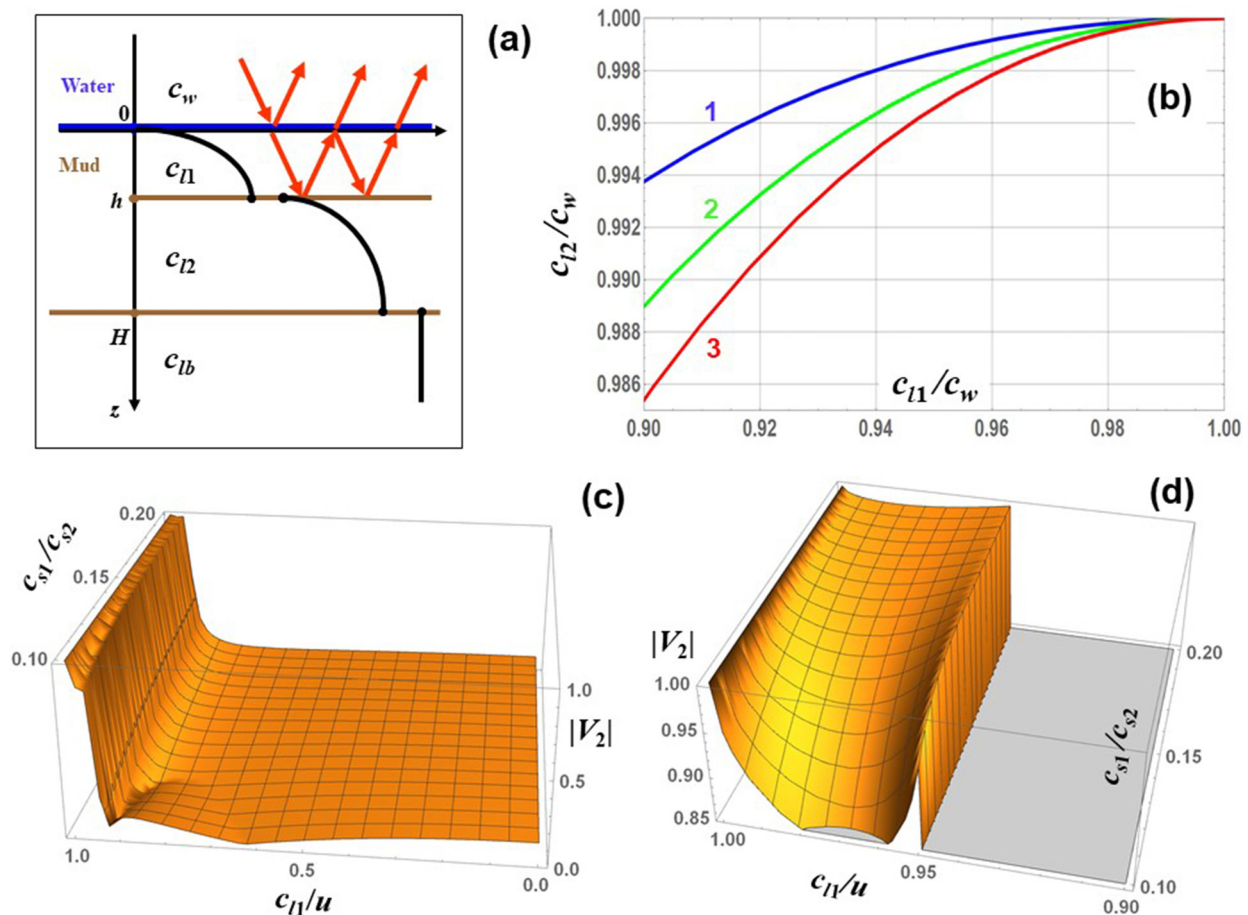

FIG. 4. (Color online) P wave resonance in a stratified seabed. (a) Geometry of resonance reflection of P waves. Arrows illustrate incident, reflected, and transmitted P waves. Constant P wave speeds in different layers are indicated in the figure. A sketch of the depth dependence of the shear speed is shown for orientation. (b) Relation between the P wave speeds in the upper ($0 < z < h$) and lower ($h < z < H$) clay layers as derived from the observed resonance frequency for three values of the ratio ρ_w/ρ_1 of densities of the water and of the upper clay layer: 0.537 (1), 0.75 (2), and 0.9 (3). (c) Absolute value of the reflection coefficient V_2 of plane P waves from interface $z = h$ of two solids with compressional speeds $c_{l1} < c_{l2}$ and shear speeds $c_{s1} < c_{s2}$. The wave is incident from the solid with the smaller wave speed. In the figure, $c_{l1}/c_{l2} = 0.95$, $c_{l1}/c_{s1} = 20$, and the ratio of densities of the two solids $\rho_2/\rho_1 = 1.2$. The angle of incidence θ_l is related to the trace velocity u of the wave by the equation $\sin\theta_l = c_{l1}/u$. (d) An expanded view of the part of figure (c) at $|V_2| > 0.85$ and $0.9 < c_{l1}/u < 1$.

and V_2 do not exceed unity. For the condition in Eq. (20) to be met, $|V_1|$ and $|V_2|$ should be equal to 1 simultaneously. The reflection coefficient of a plane sound wave in fluid from a solid half-space is[23]

$$V_2 = \frac{Z_l \cos^2 2\theta_s + Z_s \sin^2 2\theta_s - Z}{Z_l \cos^2 2\theta_s + Z_s \sin^2 2\theta_s + Z}. \tag{21}$$

Here Z_s and Z_l are impedances of shear and P waves at $z > h$; Z is the impedance of P waves at $0 < z < h$; and θ_s is the angle that wave vector of the shear wave, below the interface, makes with the normal to the interface $z = h$:

$$\theta_s = \arcsin\frac{c_{s2}}{u}, \quad Z_s = \frac{\rho_2 c_{s2}}{\cos\theta_s},$$
$$Z_l = \frac{\rho_2 c_{l2}}{\sqrt{1 - c_{l2}^2/u^2}}, \quad Z = \frac{\rho_1 c_{l1}}{\sqrt{1 - c_{l1}^2/u^2}}. \tag{22}$$

For a propagating P wave incident on a solid half-space with a shear speed smaller than compressional speed c_{l1}, θ_s and impedances Z and Z_s are real and positive according to Eq. (22). Then, it follows from Eq. (21) that $|V_2| < 1$ unless $u = c_{l2}$. When $u = c_{l2}$, impedance Z_l is infinite, and $V_2 = 1$. This property of the reflection coefficient has a simple physical meaning. Acoustic waves cannot be totally reflected from the solid half-space because a part of the incident energy is carried away from the boundary by shear waves in the solid. The only exception occurs when the impedance of the refracted P wave in the solid becomes infinite at $u = c_{l2}$, and the amplitude of the shear wave vanishes.[23]

The condition $|V_1| = 1$ will be satisfied at $u = c_{l2}$ provided

$$c_{l1} < c_{l2} < c_w. \tag{23}$$

This inequality ensures that the plane wave is totally reflected at the fluid-fluid interface $z = 0$. The reflection coefficient from the top boundary of the layer, for incidence from below, is

$$V_1 = \exp\left[-2i\arctan\left(\frac{\rho_1}{\rho_w}\sqrt{\frac{1 - u^2 c_w^{-2}}{u^2 c_{l1}^{-2} - 1}}\right)\right] \tag{24}$$

at total internal reflection.[23] Hence, the resonance condition in Eq. (20) will be met at frequencies $f_{l,j}$ that satisfy the following equation:

$$\frac{2f_{l,j}h}{c_{l2}}\sqrt{\frac{c_{l2}^2}{c_{l1}^2} - 1} - \frac{1}{\pi}\arctan\left(\frac{\rho_1}{\rho_w}\sqrt{\frac{1 - c_{l2}^2 c_w^{-2}}{c_{l2}^2 c_{l1}^{-2} - 1}}\right) = j,$$
$$j = 0, 1, 2, \ldots. \tag{25}$$

The above derivation of the resonance conditions in Eqs. (23) and (25) extends an earlier discussion by Duncan et al.[37] of frequencies with sharply reduced transmission losses in an underwater waveguide with a homogeneous solid bottom, when the sound speed in water is larger than

the shear wave speed and smaller than the P wave speed in the bottom. The fluid-fluid boundary at $z = 0$ in our problem reduces to a pressure release boundary in the limit $\rho_w \to 0$. In this limiting case, the arctangent in Eq. (25) is replaced with $\pi/2$, and our result reduces to that of Ref. 37. When $\rho_w \to 0$, $|V_1| = 1$ at all incidence angles and for any c_w, and the requirement $c_{l2} < c_w$ in Eq. (23) does not apply.

The lowest-frequency P wave resonance corresponds to $j = 0$ in Eq. (25) and occurs at the frequency

$$f_{l,0} = \frac{c_{l2}}{2\pi h\sqrt{c_{l2}^2 c_{l1}^{-2} - 1}}\arctan\left(\frac{\rho_1}{\rho_w}\sqrt{\frac{1 - c_{l2}^2 c_w^{-2}}{c_{l2}^2 c_{l1}^{-2} - 1}}\right). \tag{26}$$

Subsequent resonances are equally spaced in frequency with the spacing

$$f_{l,j+1} - f_{l,j} = \frac{c_{l2}}{2h\sqrt{c_{l2}^2 c_{l1}^{-2} - 1}}. \tag{27}$$

Note that the frequency difference $f_{l,j+1} - f_{l,j} > c_{l1}/2h$. Under the conditions of the North Sea experiment, where $h \approx 5.6$ m, the frequency spacing exceeds 85 Hz for all reasonable values of $c_{l1} > 1000$ m/s, and—in agreement with the observations[22]—only one resonance, $f_{l,0}$, is observed within the 2–60 Hz frequency band of the source.

With the resonance frequency $f_{l,0}$, layer thickness h, and sound speed in water known, Eq. (26) relates three geoacoustic parameters: P wave speeds c_{l1} and c_{l2} in two sediment layers and the ratio ρ_w/ρ_1 of water and sediment layer densities [Fig. 4(b)]. The value $\rho_w/\rho_1 = 0.537$ has been obtained from the interface wave data (Table I). If c_{l2} were retrieved from, say, measured travel times of compressional head wave data,[38,39] c_{l1} could be unambiguously determined from Eq. (26), and vice versa. In the North Sea experiment, the nondimensional parameter $f_{l,0}h/c_w \approx 0.14$ is small. Then, Eq. (26) provides a strong constraint on deviations of the ratios c_{l1}/c_w and especially c_{l2}/c_w from unity [Fig. 4(b)]. The findings that c_{l1} and c_{l2} are smaller than but close to the sound speed in water are consistent with the available geologic information about surficial sediments[30] and expectations for P wave speeds in soft clays.[7,18,36]

In the above discussion, we modeled the top sediment layer $0 < z < h$ as a fluid. To justify the application of the fluid-solid model to the interface $z = h$ between sediment layers, it should be noted first that the layer thickness $h = 5.57$ m is small compared to the P wave wavelength $c_{l1}/f_p \sim 40$ m. For P waves, the upper layer will act as a homogeneous layer with some effective (averaged) parameters. Given the very fast relative variations of the shear rigidity with depth and that shear rigidity is extremely small in the upper part of the layer, the effective shear speed will be much smaller than the 73 m/s shear speed just above the boundary $z = h$. Similarly, the shear modulus increases by the factor of ~20 over the first 40 m below the boundary (see Table I). In a homogeneous half-space model of the

J. Acoust. Soc. Am. **149** (1), January 2021

Godin et al.   57

sediments at $z > h$, the effective shear speed should be considerably larger than the 85 m/s value just below the interface as given by the geoacoustic inversion of the interface wave data. Hence, reflection of P waves from the boundary $z = h$ should be treated as reflection at a solid-solid interface with a large contrast in shear speeds.

Figure 4(c) illustrates the angular dependence of the reflection coefficient V_2 of a plane P wave from the interface of two homogeneous solids with a large contrast between shear speeds ($c_{s2} \gg c_{s1}$). The wave is incident from the solid with a smaller shear and compressional speeds ($c_{l2} > c_{l1}$). Incidence angle θ_l of the wave is related to the trace velocity u by the equation $\sin\theta_l = c_{l1}/u$. The reflection coefficient is calculated using Eqs. (4.2.8), (4.2.13)–(4.2.15) in Ref. 23. The equations are exact but cumbersome and will not be reproduced here. V_2 is real-valued at $0 \leq u \leq c_{l2}$ and positive at $u = c_{l2}$. Note that $|V_2|$ is relatively small at steep and moderate incidence angles and, just like reflection coefficient Eq. (21) from a fluid-solid interface, has a sharp maximum at $u = c_{l2}$ [Figs. 4(c) and 4(d)]. The value of $|V_2(u = c_{l2})|$ is close to unity, and the sharp local maximum of $|V_2|$ leads to resonance reflection of P waves from the layer $0 < z < h$ at the frequencies satisfying Eq. (25) as in the case of reflection from a fluid layer between fluid and solid half-spaces. In this model, the sharpness of the observed resonance peaks [see Fig. 1(a)] is related to the sharpness of the angular dependence of the reflection coefficient around its local maximum at $u = c_{l2}$ in Fig. 4(d).

When the layer $0 < z < h$ has small but finite shear rigidity, the reflection coefficient V_1 from the upper boundary $z = 0$ of the layer deviates from the reflection coefficient Eq. (24) at a fluid-fluid interface. The reflection coefficient of P waves in a solid at the solid-fluid interface is

$$V_1 = \frac{Z - Z_l \cos^2 2\theta_s + Z_s \sin^2 2\theta_s}{Z + Z_l \cos^2 2\theta_s + Z_s \sin^2 2\theta_s} \qquad (28)$$

(see, e.g., Eq. (4.2.37) in Ref. 23). The reflection coefficient is similar to that of the plane wave incident on the interface from the fluid side, Eq. (21). At boundary $z = 0$,

$$\theta_s = \arcsin\frac{c_{s1}}{u}, \quad Z_s = \frac{\rho_1 c_{s1}}{\cos\theta_s},$$
$$Z_l = \frac{\rho_1 c_{l1}}{\sqrt{1 - c_{l1}^2/u^2}}, \quad Z = \frac{\rho_w c_w}{\sqrt{1 - c_w^2/u^2}} \qquad (29)$$

in Eq. (28). When shear speed c_{s1} is small, θ_s and Z_s are proportional to the small parameter $c_{s1}/u \ll 1$. When $c_{l1} \leq u \leq c_w$, Z is purely imaginary, and it follows from Eq. (28) that $|V_1| = 1$ up to terms of the third order in c_{s1}/u; the phase of the reflection coefficient differs from its value in Eq. (24) (i.e., at $c_{s1} = 0$) by terms $O((c_{s1}/u)^2)$. Thus, deviations of V_1 from Eq. (24) are negligible.

Together with the above analysis of V_2 [Figs. 4(c) and 4(d)], these findings justify application of the resonance conditions Eqs. (23) and (25) in our problem.

V. DISCUSSION

Identification of the fundamental mode of P–SV interface waves as the only mode that is sensitive to sediment density has allowed us to retrieve an estimate $\rho_w/\rho_1 = 0.537$ of the density contrast between water and the sediment layer $0 < z < h$. In previous geoacoustic inversions[22,30] of the same data set, density was not retrieved. In the two density models postulated in Ref. 30 on the basis of the available geologic information at the experimental site, the density ratio $\rho_w/\rho_1 = 0.574$–0.583, if the average of density in the upper 6 m of the sediments is taken for ρ_1. These values are close to the value retrieved in Sec. II C and are within the uncertainty interval of that estimate, see Table I.

Similarly, depth-independent P wave speed $c_l = c_w$ in the seabed was postulated in Ref. 30. In Ref. 22, interface wave dispersion curves were found to be insensitive to the compressional speed, which was also assumed to be depth-independent. The relatively small deviations of c_{l1} and c_{l2} from c_w that are derived in Sec. IV from the measured frequency of the P wave resonance, are consistent with the rough depth-independent models.[22,30] Furthermore, the power spectrum data provides strong constraints on variations of the P wave speed across the seafloor and within top sediment layers [Fig. 4(b)].

Inversion of the interface wave dispersion data is accomplished in Sec. II C by representing the upper 40–50 m of the seabed by two layers with power-law profiles of the shear speed. The model is motivated by the observation of two distinct slopes in log-log representation of the dispersion curves [Fig. 1(b)]. To assess this shear-speed model, it is compared here to several alternative geoacoustic models of soft marine sediments. We have considered three additional models of the shear speed depth dependence: single power-law layer, three power-law layers, and two power-law layers on top of a homogeneous half-space. In the last two models, $c_s(z) = a_2 z^{\nu_2}$ at $h < z < H$. Below the bottom of the second layer, at $z > H$, $c_s(z) = a_3 z^{\nu_3}$ in the three-layer model; in the two-layer plus half-space model, the shear speed and density in the half-space are $c_{sb} = N a_2 H^{\nu_2}$ and $\rho_b = M\rho_2$. Parameters M and N have the same meaning as in Eq. (14).

In the single-layer model, we have used the more accurate theoretical dispersion Eqs. (17)–(19) for all modes. In conjunction with the other models, Eqs. (18) and (19) have been used for the fundamental ($n = 0$) P–SV mode and SH mode 1, implying that those modes interact only with the uppermost layer; the WKB approximation has been used for all other modes. The P–SV mode 1 data is not well described by the WKB approximation and therefore does not have a good fit for any model. It might have been useful to exclude that data from the fit, but that has not been attempted.

Results of the interface wave data inversion in the alternative geoacoustic models are summarized in Table II and illustrated in Fig. 5. Ninety-five percent confidence bounds are given in Table II for parameters of the retrieved power-

TABLE II. Alternative geoacoustic models.

Parameter	Unit	Single power-law layer		Two power-law layers overlying half-space		Three power-law layers	
		Estimated value	95% Confidence Bounds	Estimated value	95% Confidence Bounds	Estimated value	95% Confidence Bounds
ρ_w/ρ_1	—	0.624	(0.446, 0.795)	0.537	(0.478, 0.596)	0.535	(0.475, 0.593)
h	m	—	—	5.57	(5.02, 6.11)	5.68	(5.25, 6.11)
a_1 (1 m)^{v_1}	m/s	39.0	(38.46, 39.58)	46.3	(46.0, 46.7)	46.3	(46.0, 46.7)
v_1	—	0.556	(0.5475, 0.564)	0.288	(0.276, 0.301)	0.288	(0.277, 0.300)
a_2 (1 m)^{v_2}	m/s	—	—	24.4	(22.5, 26.3)	28.9	(22.5, 26.3)
v_2	—	—	—	0.710	(0.677, 0.743)	0.634	(0.580, 0.688)
H	m	—	—	44.68	—	19.6	(15.75, 23.4)
M	—	—	—	2.56	—	—	—
N	—	—	—	1.185	—	—	—
a_3 (1 m)^{v_3}	m/s	—	—	—	—	24.9	(−16.0, 65.8)
v_3	—	—	—	—	—	0.710	(0.677, 0.742)

law dependencies. The two-layer model [Figs. 3(a) and 3(b)] shows major improvement over the one-layer model [Figs. 5(a) and 5(b)] in fitting the data. This is reflected in the R^2 values for the inversions, which increase from 0.966 for the one-layer model to 0.980 for the two-layer model. The difference in the R^2 values represents a decrease of the model-data misfit variance by the factor of 1.7 in the two-layer model. Comparison of Figs. 5(a)–5(b) and 3(a)–3(b) demonstrates that the one-layer model fails to fit the data at phase speeds below 75–80 m/s. The data-model mismatch is so big [Figs. 5(a)–(b)] that R^2 values calculated for the fundamental P-SV mode, −1.10, and the first SH mode, −3.07, prove to be negative. In contrast, the two-layer model adequately approximates the low-order mode data, with R^2 of 0.966 and 0.926 for the fundamental P-SV mode and the first SH mode, respectively.

The physics behind the difficulties that the one-layer model has with low-order modes can be traced back to the fact that dispersion of a slow interface wave is most sensitive to the shear speeds at depths around the turning point (Sec. III A). Parameters of the optimum one-layer model are primarily controlled by properties of the second layer ($z > h$), where turning points are located for most modes in the dataset. At phase speeds below 76 m/s, the turning points are located in the top layer, $0 < z < h$, and the mismatch between the data and one-layer model reflects the difference between the parameters of the two sediment layers.

The two-layer plus half-space model had the same R^2 and produced identical estimated values of parameters of the layers and extremely close confidence intervals of these parameters (Table II) as the two-layer model (Table I), suggesting that the data does not contain the wave frequencies
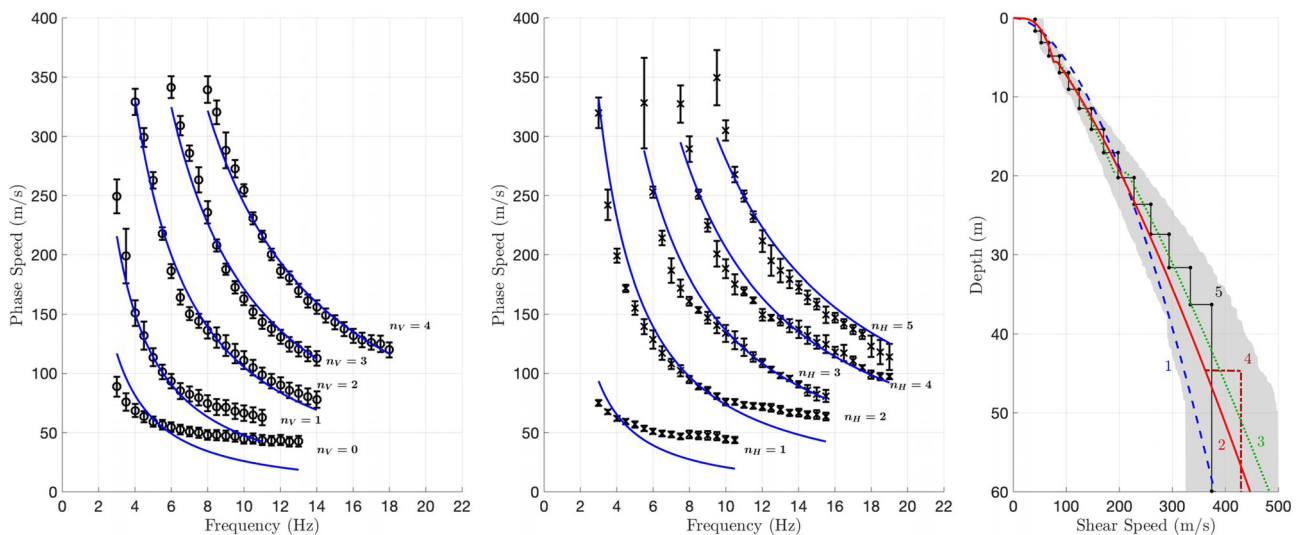

FIG. 5. (Color online) Inversion of measured dispersion curves of the interface waves for the shear-speed profile in alternative geoacoustic models. (a) Comparison of the theoretical frequency dependence of the phase speeds of interface waves in the optimum single-layer model (solid lines) with measured phase speeds of P–SV interface waves. Error bars of measurements (Ref. 22) are shown. (b) Same for measured phase speeds of SH interface waves. Mode orders n_H and n_V of, respectively, horizontally and vertically polarized interface waves are shown in the figure. Note much poorer data-model agreement than in the two-layer inversion illustrated in Figs. 3(a) and 3(b). (c) Comparison of the results of alternative single-layer (1), two-layer (2), three-layer (3), and two-layer plus half-space (4) power-law inversions with an inversion in terms of a large number of homogeneous layers (Ref. 22) (5). The shaded region is the overlap of 95% confidence intervals of the shear speed profile as obtained in Ref. 22 from the separate Bayesian inversions of the dispersion curves of the horizontally and vertically polarized interface waves.

and mode orders that interacted with the seabed below the bottom of the second power-law layer. Despite an increase in the number of degrees of freedom, the three-layer model does not noticeably improve the dispersion data fit ($R^2 =$ 0.981) and shows very low sensitivity to parameters of the deepest layer, as reflected in the confidence intervals for H, ν_3, and especially a_3. We conclude that the two-layer model is in the best agreement with available dispersion data.

We have also considered a more general two-layer model, where non-zero values of the parameter z_0 in Eq. (2) are allowed, and z_0 is considered as an additional unknown geoacoustic parameter. Despite an increase in the number of degrees of freedom, no noticeable improvement in the model-data fit was found compared to the original two-layer geoacoustic model in Table I.

A Bayesian multi-layer shear-speed inversion of the interface wave dispersion data was developed by Dong et al.[22] and considered as an approximation to the linear shear speed profile in a layer overlying a homogeneous half-space. The multi-layer model[22] ensures an excellent fit to the measured dispersion curves but its interpretation as an approximation to a linear profile is questionable. Sediments with linear ($\nu_1 = 1$) profile, unlike power-law profiles with $0 < \nu_1 < 1$, support neither SH nor slow P–SV interface waves.[9,17] This can be traced back to the fact that, when $\nu_1 \geq 1$, shear speed decreases so fast near $z = 0$ that shear wave travel time to the seafloor becomes infinite, the waves experience extraordinary attenuation and never reach the seafloor.

The results of the multi-layer shear-speed inversion[22] are compared to results of various simple, power-law-based inversions in Figs. 3(c) and 5(c). (Inversion results are extended to the 60-m depth below the seafloor, as in Ref. 22, although these may be only supported by data up to about the 45-m depth.) The results of power-law inversions, except the single-layer inversion, do not deviate far from the multi-layer geoacoustic model in the top 50 m of the seabed. The two-layer, two-layer plus half-space, and three-layer models are all well within the 95% confidence intervals[22] of the Bayesian multi-layer inversions for SH and P–SV waves. Thus, the three simple models and particularly the physics-guided, parsimonious two-layer inversion provide a shear-speed depth dependence, which is arguably as consistent with the data as the much more sophisticated and computationally intensive multi-parameter, multi-layer Bayesian inversion.

VI. CONCLUSION

Soft surficial sediments support a rich set of slow interface waves, which can account for the bulk of seismo-acoustic energy near the seafloor at low frequencies (between about 1 and a few 10s of Hertz) and are sensitive to the magnitude and depth-dependence of shear rigidity. Hydrophone measurements miss most of the interface waves. Vector sensors, such as tri-axial, bottom coupled accelerometers, are necessary to capture, separate different

polarizations, and identify various interface wave modes and other components of the full wave field.

The linear dependence between logarithms of the phase (or group) speeds of the interface waves and their frequency was proposed by Chapman and Godin[10,17] as means to identify a seabed with a power-law shear-speed profile and determine its parameters. In this paper, that simple, physics-based approach to geoacoustic inversions is extended to seabeds containing several layers of soft sediments of different composition. In application to interface wave dispersion data obtained in the North Sea off Norway, the approach leads to a low-parameter model of the shear speed profile as power-law dependences in two layers. The model provides a good fit to the data and agrees with the results of a much more elaborate Bayesian inversion.[22] In addition, a boundary between soft sediment layers is detected and sediment density is evaluated, with the result being consistent with available geologic information.

We identified a physical mechanism, which can lead to P wave resonances in stratified soft sediments, and demonstrated that the proposed mechanism can explain sharp peaks of the observed power spectra of the vertical and radial components of the particle velocity. The P wave resonance with a high quality factor is made possible by the fact that amplitudes of converted shear waves, which would otherwise take energy from and attenuate the P wave at reflection from a fluid-solid or solid-solid interface, are strongly suppressed at a particular incidence angle.

The simple, physics-guided approach presented in this paper results in a geoacoustic model that offers a consistent interpretation and a quantitative description of various salient features of the available data of the 2007 shear-wave experiment in the North Sea.

ACKNOWLEDGMENTS

[1]F. Gassmann, "Elastic waves through a packing of spheres," Geophysics 16, 673–685 (1951).
[2]J. D. Goddard, "Nonlinear elasticity and pressure-dependent wave speeds in granular media," Proc. R. Soc. London Ser. A: Math. Phys. Sci. 430(1878), 105–131 (1990).
[3]S. N. Domenico, "Elastic properties of unconsolidated porous sand reservoirs," Geophysics 42(7), 1339–1368 (1977).
[4]E. I. Hamilton, "Attenuation of shear waves in marine sediments," J. Acoust. Soc. Am. 60, 334–338 (1976).
[5]G. M. Bryan and R. D. Stoll, "The dynamic shear modulus of marine sediments," J. Acoust. Soc. Am. 83, 2159–2164 (1988).
[6]M. D. Richardson, E. Muzi, B. Miaschi, and F. Turgutcan, "Shear wave velocity gradients in near-surface marine sediments," in Shear Waves in Marine Sediments, edited by J. M. Hovem, M. D. Richardson, and R. D. Stoll (Kluwer, Dordrecht, 1991), pp. 295–304.
[7]J. C. Osler and D. M. F. Chapman, "Seismo-acoustic determination of the shear-wave speed of surficial clay and silt sediments on the Scotian shelf," Canadian Acoustics 24(4), 11–22 (1996), available at https://jcaa.caa-aca.ca/index.php/jcaa/article/view/106.

60   J. Acoust. Soc. Am. 149 (1), January 2021

Godin et al.

[8]F. A. Bowles, "Observations on attenuation and shear-wave velocity in fine-grained, marine sediments," J. Acoust. Soc. Am. **101**, 3385–3397 (1997).

[9]O. A. Godin and D. M. F. Chapman, "Shear speed gradients and ocean seismo-acoustic noise resonances," J. Acoust. Soc. Am. **106**(5), 2367–2382 (1999).

[10]D. M. F. Chapman and O. A. Godin, "Dispersion of interface waves in sediments with power-law shear speed profiles. II: Experimental observations and seismo-acoustic inversions," J. Acoust. Soc. Am. **110**, 1908–1916 (2001).

[11]K. Ohta, S. Matsumoto, K. Okabe, K. Asano, and Y. Kanamori, "Estimation of shear wave speed in ocean-bottom sediment using electro-magnetic induction source," IEEE J. Ocean. Eng. **33**(3), 233–239 (2008).

[12]J. Dettmer, S. E. Dosso, and J. C. Osler, "Bayesian evidence computation for model selection in non-linear geoacoustic inference problems," J. Acoust. Soc. Am. **128**, 3406–3415 (2010).

[13]H. Dong and S. E. Dosso, "Bayesian inversion of interface-wave dispersion for seabed shear-wave speed profiles," IEEE J. Oceanic Eng. **36**(1), 1–11 (2011).

[14]M. M. Haney and V. C. Tsai, "Nonperturbational surface-wave inversion: A Dix-type relation for surface waves," Geophysics **80**(6), EN167–EN177 (2015).

[15]A. G. Soloway, P. H. Dahl, and R. I. Odom, "Modeling explosion generated Scholte waves in sandy sediments with power law dependent shear wave speed," J. Acoust. Soc. Am. **138**, EL370–EL374 (2015)..

[16]E. Cunningham and V. Lekic, "Constraining properties of sedimentary strata using receiver functions: An example from the Atlantic Coastal Plain of the southeastern United States," Bull. Seismol. Soc. Am. **110**, 519–533 (2020)..

[17]O. A. Godin and D. M. F. Chapman, "Dispersion of interface waves in sediments with power-law shear speed profiles. I: Exact and approximate analytical results," J. Acoust. Soc. Am. **110**, 1890–1907 (2001).

[18]D. Jackson and M. Richardson, High-Frequency Seafloor Acoustics (Springer, New York, 2007).

[19]D. Rauch, "Experimental and theoretical studies of seismic interface waves in coastal waters," in Bottom-Interacting Ocean Acoustics, edited by W. A. Kuperman and F. B. Jensen (Plenum, New York, 1980), pp. 307–327.

[20]J. Ewing, J. A. Carter, G. H. Sutton, and N. Barstow, "Shallow water sediment properties derived from high-frequency shear and interface waves," J. Geophys. Res.: Solid Earth **97**(B4), 4739–4762, https://doi.org/10.1029/92JB00180 (1992).

[21]G. Nolet and L. M. Dorman, "Waveform analysis of Scholte modes in ocean sediment layers," Geophys. J. Int. **125**(2), 385–396 (1996).

[22]H. Dong, T.-D. Nguyen, and K. Duffaut, "Estimation of seabed shear-wave velocity profiles using shear-wave source data," J. Acoust. Soc. Am. **134**, 176–184 (2013).

[23]L. M. Brekhovskikh and O. A. Godin, Acoustics of Layered Media. 1: Plane and Quasi-Plane Waves. 2nd ed. (Springer, Berlin, 1998), pp. 14–29, 87–98, 183–186, 218–226.

[24]A. Caiti, T. Akal, and R. D. Stoll, "Estimation of shear wave velocity in shallow marine sediments," IEEE J. Ocean. Eng. **19**, 58–72 (1994).

[25]S. A. Frivik, R. Allnor, and J. M. Hovem, "Estimation of shear wave properties in the upper seabed using seismo-acoustical interface waves," in High Frequency Acoustics in Shallow Water, edited by N. G. Pace, E. Pouliquen, O. Bergem, and A. P. Lyons (SACLANTCEN, La Spezia, Italy, 1997), pp. 155–162.

[26]S. E. Crocker, J. H. Miller, G. R. Potty, J. C. Osler, and P. C. Hines, "Nonlinear inversion of acoustic scalar and vector field transfer functions," IEEE J. Ocean. Eng. **37**(4), 589–606 (2012).

[27]J. Shi, S. E. Dosso, D. Sun, and Q. Liu, "Geoacoustic inversion of the acoustic-pressure vertical phase gradient from a single vector sensor," J. Acoust. Soc. Am. **146**(5), 3159–3173 (2019).

[28]P. H. Dahl and D. R. Dall'Osto, "Estimation of seabed properties and range from vector acoustic observations of underwater ship noise," J. Acoust. Soc. Am. **147**(4), EL345–EL350 (2020).

[29]M. Vanneste, C. Madshus, V. L. Socco, M. Maraschini, P. M. Sparrevik, H. Westerdahl, K. Duffaut, E. Skomedal, and T. I. Bjørnarå, "On the use of the Norwegian Geotechnical Institute's prototype seabed-coupled shear wave vibrator for shallow soil characterization. I. Acquisition and processing of multimodal surface waves," Geophys. J. Int. **185**, 221–236 (2011).

[30]V. L. Socco, D. Boiero, M. Maraschini, M. Vanneste, C. Madshus, H. Westerdahl, K. Duffaut, and E. Skomedal, "On the use of the Norwegian Geotechnical Institute's prototype seabed-coupled shear wave vibrator for shallow soil characterization. II. Joint inversion of multimodal Love and Scholte surface waves," Geophys. J. Int. **185**, 237–252 (2011).

[31]S. C. Webb, "Broadband seismology and noise under the ocean," Rev. Geophys. **36**(1), 105– 142, https://doi.org/10.1029/97RG02287 (1998).

[32]R. A. Stephen, F. N. Spiess, J. A. Collins, J. A. Hildebrand, J. A. Orcutt, K. R. Peal, F. L. Vernon, and F. B. Wooding, "Ocean seismic network pilot experiment," Geochem. Geophys. Geosyst. **4**(10), 1092 (2003).

[33]A. P. Prudnikov, Y. A. Brychkov, and O. I. Marichev, Integrals and Series, Volume 1: Elementary Functions (Gordon & Breach Sci. Publ., New York, 1986).

[34]1. M. Abramovitz and I. A. Stegun (eds.), Handbook of Mathematical Functions with Formulas, Graphs, and Tables, Appl. Math. Ser., Vol. 55 (Dover Publications, New York, 1972), pp. 253–293, 555–585.

[35]K. Aki and P. G. Richards, Quantitative Seismology. 2nd ed. (Univ. Science Books, Sausalito, 2002), pp. 249–254.

[36]E. L. Hamilton, "Sediment sound velocity measurements made in situ from bathyscaph Trieste," J. Geophys. Res. **68**(21), 5991–5998, https://doi.org/10.1029/JZ068i021p05991 (1963).

[37]A. J. Duncan, A. N. Gavrilov, R. D. McCauley, I. M. Parnum, and J. M. Collis, "Characteristics of sound propagation in shallow water over an elastic seabed with a thin cap-rock layer," J. Acoust. Soc. Am. **134**(1), 207–215 (2013).

[38]O. A. Godin, N. R. Chapman, M. C. A. Laidlaw, and D. E. Hannay, "Head wave data inversion for geoacoustic parameters of the ocean bottom off Vancouver Island," J. Acoust. Soc. Am. **106**(5), 2540–2551 (1999).

[39]J. Li, P. Gerstoft, M. Siderius, and J. Fan, "Inversion of head waves in ocean acoustic ambient noise," J. Acoust. Soc. Am. **147**(3), 1752–1761 (2020).